Terahertz metamaterial absorbers with fixed, controllable, and tunable multiband characteristics

BALU ASHVANTH[1,*], BACTAVATCHALAME PARTIBANE[2]
[1]*Dept. of ECE, Vel Tech Rangarajan Dr. Sagunthala R&D Institute of Science and Technology, Chennai-62, India*
[2]*Dept. of ECE, Sri Sivasubramaniya Nadar College of Engineering, Chennai-110, India*

This article presents three terahertz absorbers with Fixed, Controllable, and Tunable multiband using miniaturized metamaterial unit cells. The first absorber uses a spiral layer made of copper at the top which realizes five absorption bands from 0.1THz to 1THz. The unit cell size is minimized to λ/15.5 by using an interconnected quadrant structure. Due to the fourfold symmetry, the absorber is polarization insensitive. The second absorber consists of five arcs-based resonator. The simulation results show that the structure has five distinct absorption peaks between 0.1THz to 2THz, each with an absorption of over 90% Moreover; this design gives considerable freedom for shifting the frequencies of the absorber by varying the arc lengths. The effect of the spacing of arcs on the positioning of the individual band is analyzed. The third THz absorber functionality is improved by including a tuning mechanism. It uses a convoluted meandered line design at the top to achieve five band resonances between 0.1THz and 5THz. To enhance the bandwidth coverage, the lower four bands are made tunable by using graphene material at the spacings of the patch. The absorption peaks were raised above 95% on all the operating bands which makes it a perfect candidate to be used for sensing applications.

(Received August 11, 2022; accepted April 5, 2023)

Keywords: Absorber, Tuning, Multiband characteristics, Metamaterial

1. Introduction

Terahertz absorbers are finding new applications both in the military and civilian sectors. Due to this, constant efforts have been made worldwide to enhance the performance of these absorbers. A coherent absorber was reported in [1] which regulates the absorption rate of strong waves with weak waves by utilizing gain material behind the substrate. However, the asymmetric design of the unit cell resulted in angular and polarization instability to the incident waves. The researchers in [2] proposed a miniaturized narrowband absorber with three metallic layers separated from each other using low-loss cyclic olefin copolymer as dielectric spacers. However, variation of the absorption response at 0.5THz for different incident angles was observed and it happened because of a change in the capacitance of the patch arrays for various incident angles.

A wide band absorber covering frequency from 0.65 to 3.03 THz was implemented in [3]. A graphite sheet placed in the dielectric cavity provides mixed modes for achieving wideband absorption. However, the usage of multiple dielectric layers enlarges the absorber volume which impacts its compactness. All-dielectric metasurface THz absorbers (AMTAs) device was reported in [4] which uses a single-layer all-silicon array as a patch whose absorption frequency changes with a refractive index of the surrounding medium. The research work literature [5] consists of graphene-based square split-ring resonator arrays in the unit cell. The four tunable graphene-based chiral metamaterial absorbers with a different number of absorption bands were demonstrated along with the tuning mechanism. However, in the above works, the unit cell uses a simple and traditional design that maximizes the absorber dimension, thus making it less effective for the specified application. A five-band absorber based on a patterned four-gap comb resonator and a metallic board separated by a dielectric layer is presented in [6]. It combines the resonance of various-sized sub-units into a coplanar super-unit structure or stacked layers to obtain the multi-band response. Even though the reported absorber utilizes a simple structure, due to its asymmetric design its frequency response lacks angular stability. In the literature [7] metamaterial absorber with multiband characteristics is implemented to solve the limited bandwidth problem of the internet of things backhaul network. The absorber has six L-shaped stubs with graphene at the edges to realize six tunable absorption bands. However, the absorption rate was not uniform over all the operating bands. The researchers in [8-9] presented a metamaterial composed of a layer of metallic structural and two graphene sandwich structures as well as polymer spacers. By adjusting the Fermi level of graphene, this tunable metamaterial can achieve electronically reconfigurable terahertz reflection, transmission, and absorption in a highly efficient manner. A tunable terahertz (THz) frequency selective surface (FSS) based on the metal graphene structure is shown in [10]. Even though independent frequency tunability of the triple-band is demonstrated, its structure is asymmetrical and hence only suitable for normal incidence of EM waves. A tunable broadband terahertz absorber is reported in [11]], which consists of identical vanadium dioxide (VO_2) square loops whose conductivity can be varied electrically to change the absorption rate. The research work in [12] reports two absorbers with and without frequency tuning.

The zigzag absorber produces multibands over the narrow bandwidth while the V-shaped absorber achieves multiband along the wide bandwidth with tuning capability to solve sensing-related issues. A miniaturized frequency selective surface is presented in [13] for electromagnetic shielding applications. The miniaturization was achieved by using meandered line-based triple patches which were connected together through metallic vias. In [14], [15] a dual-band terahertz (THz) absorber based on the vertical-square-split-ring structure made up of InSb and copper was proposed. Research work in [16] reported multiband absorber using pentagon-shaped resonator. However, the absorption bands are not individually controllable in the above literature.

In this paper, three absorbers with multiband characteristics showing progressive performance one after another are demonstrated. Absorber design begins with fixed Hexa bands whose center frequencies are not individually controllable. This lagging is rectified in the second design by incorporating multiple arcs in the resonator corresponding to the number of absorption bands. The length of arcs decides the position of bands. To maximize the bandwidth coverage, a tunable absorber is introduced whose bands are shifted by varying the chemical potential of graphene material. This manuscript is organized as follows: Section 1 elaborates on the design of the fixed absorber and its frequency response. Sections 2 and 3 briefs the working mechanism of controllable and tunable THz absorbers respectively.

2. Absorber with fixed bands

2.1. Unit cell design

The proposed absorber unit cell front view is shown in Fig. 1 (a). It consists of a line that is meandered along a spiral pattern in each quadrant which is covered by an L-shaped strip. The larger curvature in the spiral structure is having a radius of 38µm. Constructing this design in one quadrant and rotating 90 degrees along the Z axis gives a complete patch structure. The spiral pattern in each quadrant is connected to the L strip of the adjacent quadrant to achieve miniaturization. The designed unit cell has a patch and ground plane separated by a polyimide substrate of the thickness of 18µm as illustrated in Fig. 1 (b).

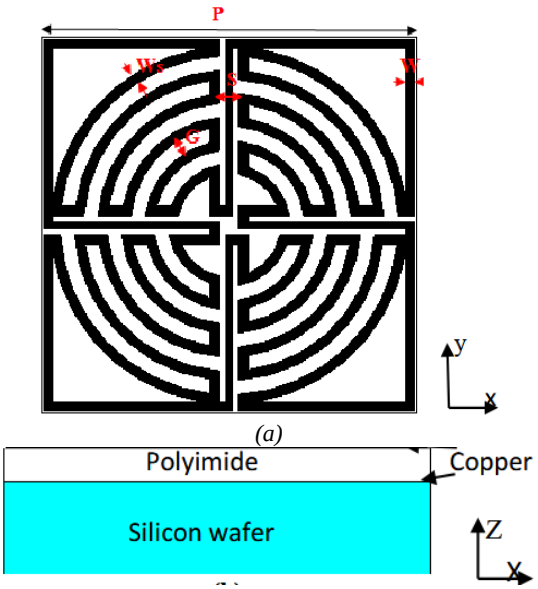

Fig. 1. Unit cell of absorber (a) Front view (b) Bottom view (color online)

Table 1. Dimensions of absorber 1.

P	W	Ws	S	G	T
80	2	2	4	3	18

All dimensions are in µm

The whole structure is backed by a silicon wafer to improve the stability of the absorber. All the geometrical parameters are chosen to fit the design inside the substrate area which is a square of 80×80 mm^2. The unit cell of the proposed metamaterial is placed along the *x-y* plane and the physical dimensions of the unit cell are of a sub-wavelength size. The dimensions are optimized to get five nearby absorption frequency bands between 0.1 to 1THz. The conducting patch and ground are made of copper whose thickness is 0.5µm.

3. Results and discussion

The electromagnetic wave is made to an incident on the unit cell surface from the +Z direction and it is linearly polarized. Here the thickness of the bottom metal layer is chosen to be larger than the skin depth and hence the incidence of electromagnetic waves gets reflected in the substrate from the top of the bottom ground plane. This unit cell realizes five bands of operation between 0.1 to 1THz which are centered at 0.24THz, 0.56THz, 0.65THz, 0.82THz, 0.95THz respectively and their corresponding absorption peaks with absorption rates are 91%, 82%, 90%, 99%, and 99% respectively as depicted in Fig. 2 (a). As shown in Fig. 2 (a), the usage of lossy polyimide as a substrate provides better absorption when compared to loss-free polyimide.

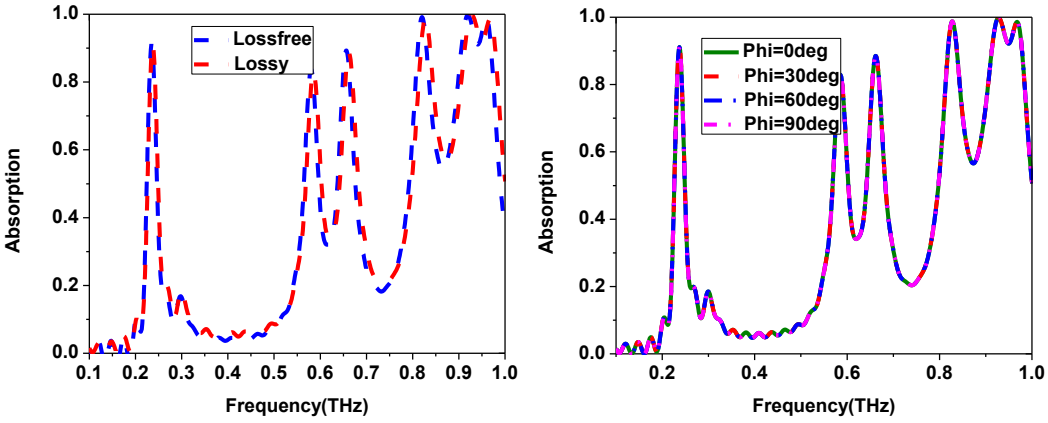

Fig. 2. Calculated absorption spectra of the proposed unit cell for (a) lossy and loss-free dielectric substrate (b) various polarization angles of the incident wave (color online)

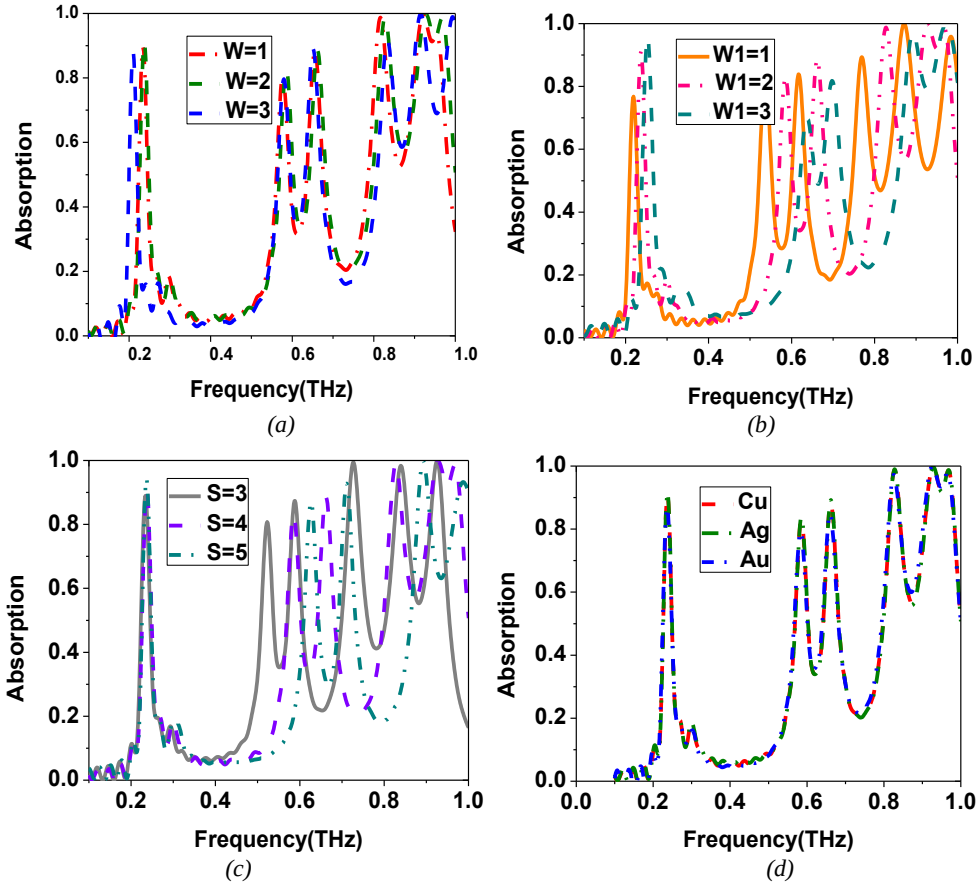

Fig. 3. Parametric studies of absorption spectra of the proposed unit cell (a) W, (b) W1, (c) S, (d) different conductors (color online)

To check the polarization insensitivity, the absorber was subjected to incident waves with different inclination angles. It is inferred from Fig. 2 (b) that the polarization state of an incident wave does not affect the absorption rate of the proposed absorber as it has a symmetric structure which is verified by changing the polarization angle from 0 to 90 degrees and keeping the incident wave oriented at 0 degrees. Parameters such as meandered line width, spacing between the quadrant structures, gap in the spiral, and the dielectric constant of the substrate can be used to carefully control the frequency response of the unit cell. The dependence of absorption spectra on various parameters of the absorber is investigated with graphs shown in Fig. 3. It can be seen from Fig. 3 (b) that the absorption bands shift towards the right side with a rising peak value when the width of the circular zigzag structure is increased. On increasing the spacing between the circular zigzag structures from 3 to 5µm, the number of absorption bands decreases as illustrated in Fig. 3 (c). Using different conducting materials namely copper (Cu),

silver (Ag), and gold (Au) for the absorber patch shows a similar response on the absorption rate as shown in Fig. 3 (d).

4. Absorber with controllable bands

4.1. Unit cell design

The conceptual view of the arc absorber is shown in Fig. 4. The absorber has four layers; which top layer is a patch made of copper. The second layer is a substrate built with polyimide dielectric of the thickness of 18µm with relative permittivity of 3.4. The copper sheet sandwiched between two dielectric acts as a ground to reflect the waves falling on it to a substrate. A silicon wafer is appended at the rear side of the absorber to offer rigidity to the design. The dimension of the unit cell is restricted to 80×80µm and it is bisected into four quadrants of size 40×40µm. Each quadrant of the unit cell has six arcs A, B, C, D, E, and F having lengths specified in angles of 280^0, 257^0, 265^0, 270^0, 290^0, and 305^0 respectively which provide six absorption bands between 0.1THz to 2THz. The radius of arcs from A to F is 38µm, 36µm, 34µm, 32µm, 30µm, and 28µm respectively. A full-wave simulation of the reported absorber was implemented using the electromagnetic simulation software CST Microwave Studio. The boundaries in the x and y direction are set as unit cells and those in the z-direction are set as open for waveguide ports to be assigned. Thus the electromagnetic waves are made to an incident on the absorber surface along the Z axis. The frequency domain solver is chosen to calculate the reflection coefficient from which the absorption coefficient has been derived. The absorption spectrum of the designed absorber is illustrated in Fig. 5. There are six bands with center frequency 0.76THz, 1.15THz, 1.28THz, 1.45THz, 1.65THz, and1.92THz existing between 01THz to 2THz and their corresponding absorption rates are 99%, 91%, 95%, 94%, 97%, and 90% respectively.

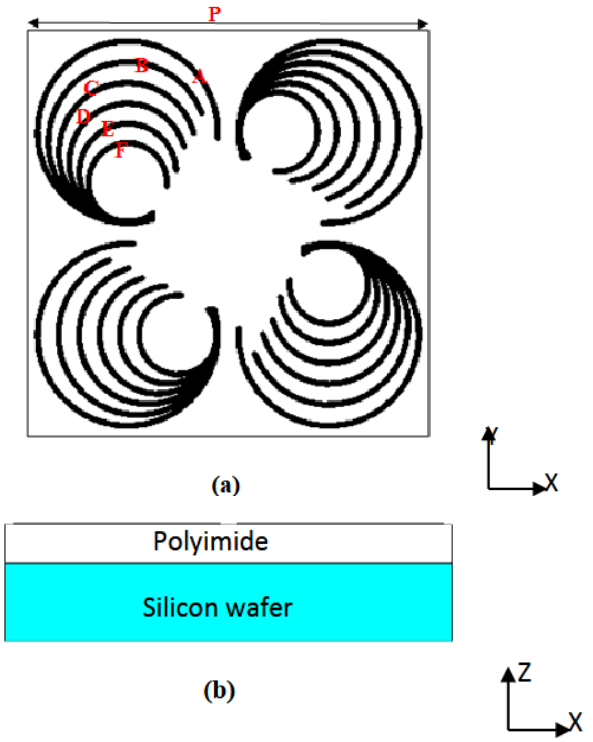

Fig. 4. Structure of proposed absorber unit cell (a) Front view (b) Bottom view (color online)

Table 2. Dimensions of absorber 2.

P	A arc	B arc	C arc	D arc	E arc	F arc	T
80	280^0	257^0	265^0	270^0	290^0	305^0	18

All dimensions are in µm

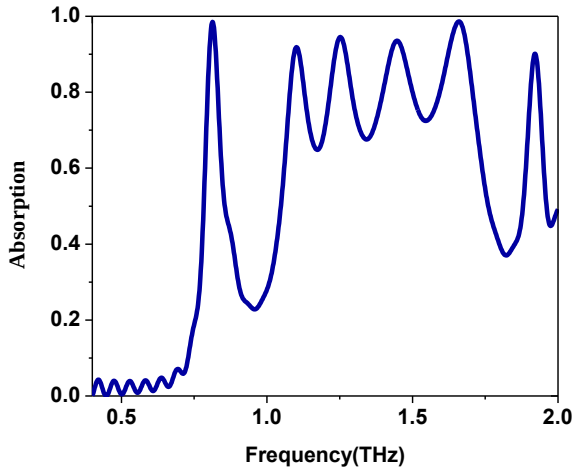

Fig. 5. Calculated absorption spectra for the proposed absorber (color online)

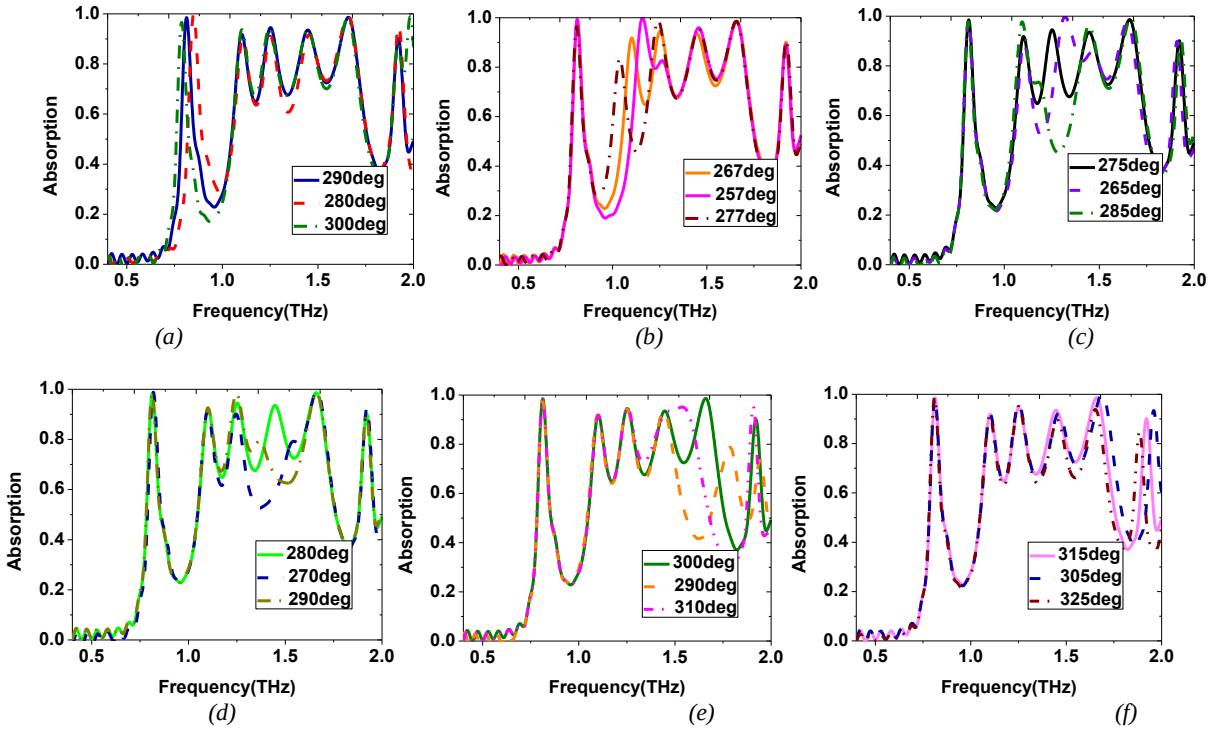

Fig. 6. Absorption band controlling by varying corresponding length of Arc a) A-0.76THz, b) B-1.15THz, c) C-1.28THz, d) D-1.45THz, e) E-1.65THz, f) F-1.92THz (color online)

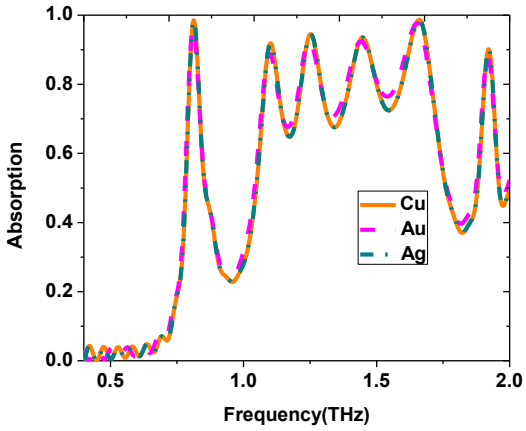

Fig. 7. Calculated absorption bands for different conductor materials (color online)

The effect of conductor material on the absorption spectra is investigated by using three different materials such as copper(Cu), Gold(Au), and Silver(Ag) having a conductivity of 0.596×10^6/cm**Ω**, 0.452×10^6/cm**Ω**, and 0.63×10^6/cm**Ω** respectively. It is observed that the performance of the absorber remains the same on using these three different conductor materials. Due to the cost-effectiveness of copper material among others, it has been chosen for the design.

4.2. Results and discussion

A study of arc lengths on the individual absorption bands is carried over to analyze the absorption spectrum and to understand the working principle of the absorber. The absorption spectra have six discrete absorption peaks located at different resonant frequencies. By varying each arc length from 250 to 325degree, the absorption peak position is varied as illustrated in Fig. 6. The arc length decides the frequency separation between individual bands and hence it needs careful selection and optimization. For band1, its resonance absorption peak is located at 0.76THz with an absorptivity of 99%. On varying the arc A length from 280° to 300°, its corresponding band1 center frequency shifts towards a lower frequency of 0.65THz from 0.91THz with absorptivity remaining almost constant as shown in Fig. 6 (a). The band 2 absorption peak is residing at 1.15THz with an absorptivity of 91%. When the arc B length is changed from 257° to 277°, band2 center frequency shows obvious shifting from 1.23THz to 1.02THz. As the resonant frequency moves down, there is a corresponding decrease in the absorption peak from 99% to 85% as depicted in Fig. 6 (b). Similarly, the shifting of resonant frequency and its absorption peaks is happening for all the other bands as illustrated in Fig. 6 (c)-(f). From all the cases it is inferred that even though, the increase in arc lengths brings miniaturization, there is a substantial reduction in the absorptivity which leads to the downfall of this absorber from using it in highly sensitive sensing applications.

To study the influence of spacing among the arc strips on the spectrum of the proposed absorber, the arc separation at the bottom origin and between adjacent quadrants is varied. From Fig. 8 (a), it is inferred that the adjacent arc spacing at the origin is zero, and there are six absorption bands. When the spacing is increased from 0 to 0.5 μm the bands are well isolated but lead to an increase in their number with a reduced absorption rate that

showcases the drawback of uncontrollable individual bands. While the distance of separation between arc structure of the adjacent quadrant reduces, the number of bands increases due to harmonics as depicted in Fig. 8 (b). It is necessary to avoid the harmonics due to their reasonable absorptivity along with the desired bands. Hence the spacing in and around the arc structure is optimized properly with the most care.

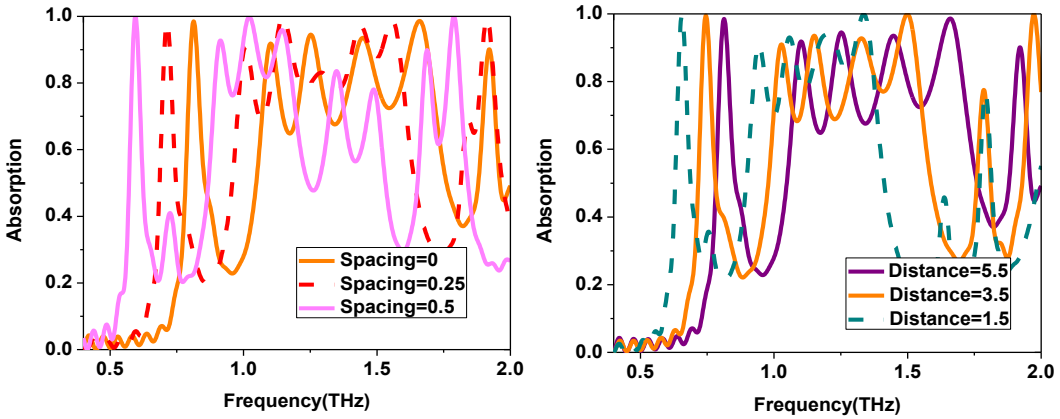

Fig. 8. Parametric study of (a) origin separation spacing between arcs, (b) Distance between adjacent arc structures in μm (color online)

5. Absorber with tunable bands

5.1. Unit cell design

The schematic of the proposed absorber is illustrated in Fig. 9. The proposed unit cell has a patch and ground plane separated by a polyimide substrate of the thickness of 13μm and a period of 41μm. The patch and ground plane are made with a copper of thickness 0.5 μm. The patch is built by a meandered line which is convoluted to form vertical and horizontal rectangular mounts as shown in the top right quadrant of the unit cell. There are four vertical mounts whose heights are adjusted to be at L1=17μm, L2=14.5μm L3=12μm, L4=9.5μm for obtaining resonance at 0.96THz, 2THz, 2.66THz, 3.75THz. The period of absorber renders the additional 4.51THz band. The four horizontal mounts are used to achieve impedance matching at the initial four bands and their heights are optimized to 2μm, 6μm, 6μm, and 2μm respectively from the top. The graphene is placed in each vertical rectangular mount for tuning its corresponding absorption band. The patch that was formed in one quadrant is rotated along the Z axis about 90 degrees to form a symmetric structure for proving angular stability to the designed absorber. The whole absorber is backed by a silicon wafer which is twice the thickness of the substrate to increase its solidity for practical use. The depth of graphene in the tunable absorber is optimized to be 4μm for getting reasonable shifts across all the operating bands while tuning.

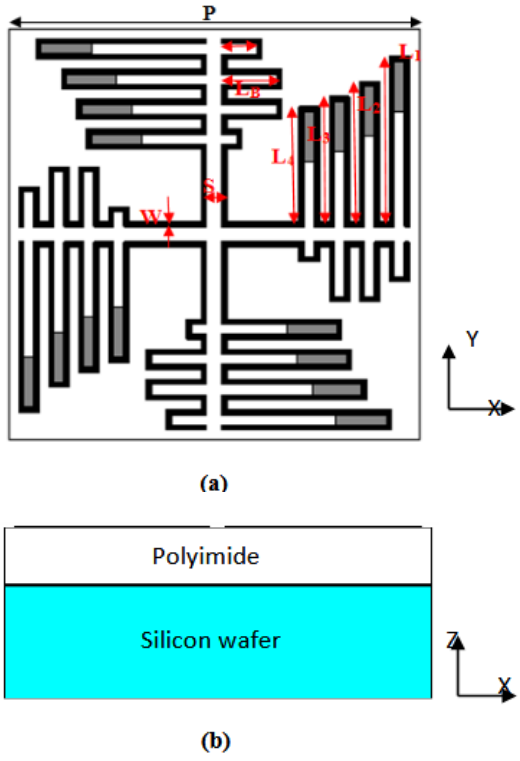

Fig. 9. Proposed Unit Cell Design (a) Front view, (b) Bottom view (color online)

Table 3. Dimensions of absorber 3

P	W	S	T	L_1	L_2	L_3	L_4	L_A	L_B
40	1	4	13	17	14.5	12	9.5	2	6

All dimensions are in μm

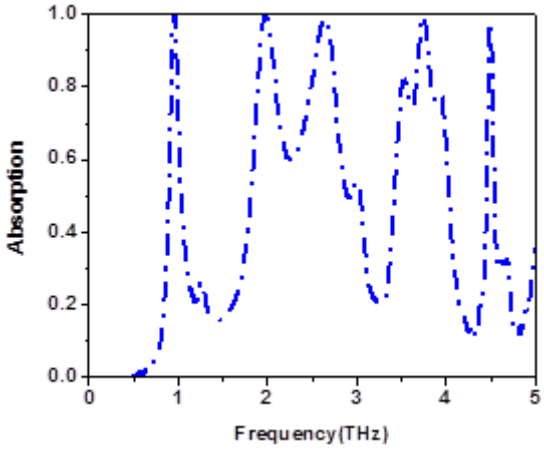

Fig. 10. Absorption coefficient of the proposed absorber (color online)

The whole structure is simulated in CST Microwave Studio to observe the absorption spectrum. The simulated absorption result of the pentaband absorber in the frequency range of 0.1–5 THz is shown in Fig. 10. By properly adjusting the dimension of this vertical convoluted line, the unit cell is made to resonate at five different frequencies of 0.96THz, 2THz, 2.66THz, 3.75THz, and 4.51THz with absorptivity of 99%, 99%, 98%, 98%, 96% respectively as illustrated in Fig. 10. The horizontal convoluted line lengths were optimized carefully to attain the maximum absorption peaks for the resonant bands. Thus the designed absorber performs perfect absorption at all the operating bands hence suitable for highly sensitive sensing applications. The full width at half maximum (FWHM) estimated from the spectrum shows a gradual increase with a decrease in the length of the convoluted rectangular mount except for the last band that is realized based on the periodicity of the absorber.

5.2. Results and discussion

If the conduction band Fermi energy of graphene is greater than half of the incident photon energy, the intraband conductivity dominates over the interband conductivity of graphene. The graphenes Fermi energy E_f can be altered by externally applied voltage V_g to the structure. The Fermi energy can be given by

$$E_f = hv_f\sqrt{\frac{\pi\epsilon_d\epsilon_o V_g}{e}} \quad (1)$$

where $v_f(10^6\ m/s)$ is the Fermi velocity, ϵ_d is the dielectric constant of the substrate, V_g is the applied chemical potential to the graphene and e is the electron charge. The conductivity of graphene is exponentially related to its Fermi energy. As Fermi energy is directly proportional to the applied voltage, conductivity increases with potential. This property of graphene makes it a perfect material to be used for tuning mechanisms.

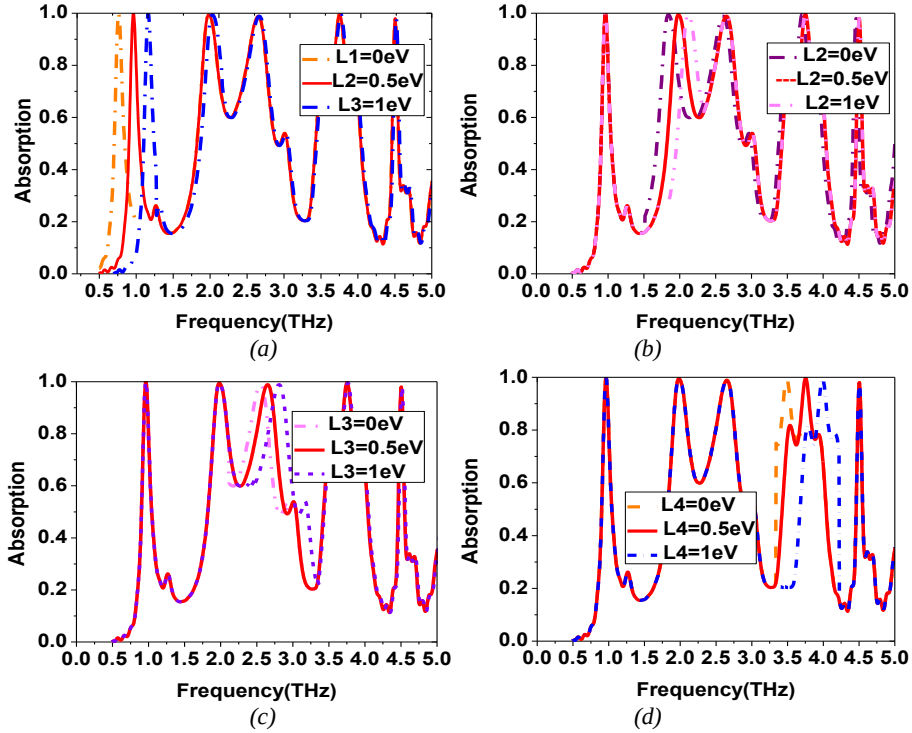

Fig. 11. Absorption spectrum by tuning of rectangle mounts graphene (a) L1-0.96THz (b) L2-2THz (c) L3-2.66THz (d) L4-3.75THz (color online)

It is found that the proposed absorber exhibits excellent frequency tuneability in four bands by adjusting the graphene chemical potentials which were attached to every vertical convoluted line. The independent frequency tuneability of the proposed pentaband absorber is demonstrated in Fig. 11. When varying the chemical potential of A graphene from 0 to 1eV by keeping other potential fixed, the center frequency of absorption band 1 shift from 0.65 to 1.22THz as shown in Fig. 11 (a). The second band shifts from 1.8THz to 2.2THz with increasing B graphenes chemical potential from 0 to 1eV while other bands remain static when their graphene potential is fixed. Similarly, the switching of resonant frequency happens for bands 2 & 3 viz 2.46THz to 2.86THz and 3.55THz to 395THz by changing the graphene C, D chemical potential from 0 to 1eV as depicted in Fig. 11 (c) and (d). Table 1 shows the comparison of the proposed works with similar literary works. It is observed that the reported absorbers have a small size, higher bandwidth coverage, more operational bands, frequency tuning, and symmetric unit cell structure.

The range of incidence angles for which the frequency response remains unchanged determines the angular stability of the proposed absorber. The angular stability is evaluated under the TE case and is presented in Fig. 12. The tunable absorber provides a stable response up to the incidence angle θ = 60°. In the first absorber, the split square loop encloses four highly convoluted zig-zag-shaped resonators distributed along with the corners of the square loop. This distribution results in rotational symmetry thereby ensuring polarization stability. As the length of the arm increases, the resonance frequency decreases, and by tri-folding the arm some additional harmonics were obtained. In the second absorber, the multiple bands can be realized by using independently controllable sub-wavelength-based resonating structures in the patch. For the third absorber, the meandered line is convoluted to form four vertical rectangular mounts. The combined effect of the localized resonance response of these sub-structures gives rise to the multiple-band absorption.

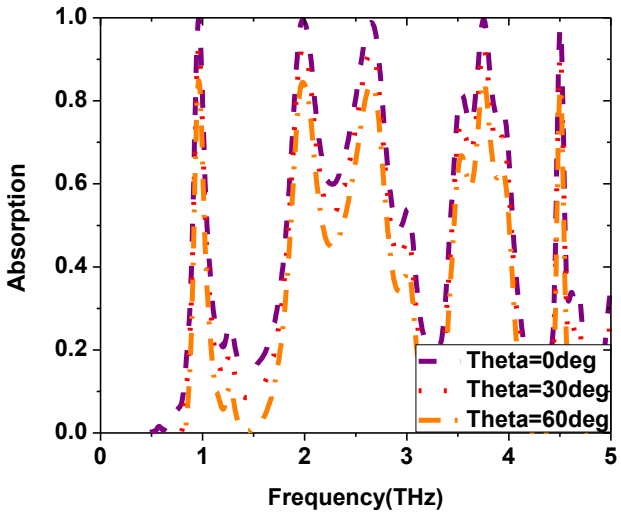

Fig. 12. Absorption spectrum for various incidence angles in TE mode (color online)

Table 4. Comparison of proposed works with literature

	Unit Cell Size (μm)	Bandwidth coverage	Number of Bands	Frequency tuning	Technique
Work1	λ/15.5	0.1 to 1THz	0.24THz, 0.56THz, 0.65THz, 0.82THz, 0.95THz	No	Interconnected spiral pattern
Work2	λ/5	0.5 to 2THz	0.76THz, 1.15THz, 1.28THz, 1.45THz, 1.65THz, 1.92THz	No	Multiple Arc structure
Work3	λ/4	0.5 to 5THz	0.96THz, 2THz, 2.66THz, 3.75THz, 4.51THz	Yes	Convoluted line & Graphene
[1]	λ/5.2	15THz to 18THz	15.25THz, 17.75THz	No	Gain material behind the substrate
[2]	λ/5.8	0.5THz	0.5THz	No	Three metallic layers
[3]	λ/4.6	0.65 to 3.03 THz	1.75THz	No	Graphite sheet between the dielectrics
[4]	λ/1.25	0.8THz to 2THz	1.2THz	No	All-dielectric metasurface

6. Conclusion

A novel method of designing terahertz multi-band absorbers based on miniaturized unit cells is demonstrated in this work. A set of THz absorbers with fixed, controllable, independent frequency tuneability was proposed and investigated numerically, with the balance between performance and tuneability achieved. The first absorber realized five absorption bands between 0.1 to 1THz whose unit cell size is reduced to $\lambda/15.5$. To achieve independent control of absorption bands, six arcs were etched in each quadrant to realize six absorption bands that lie between 0.1 to 2THz with absorptivity of more than 90% on all the operating bands. The unit cell size is reduced to $0.2\lambda \times 0.2\lambda$. The third absorber has a foot print of $0.25\lambda \times 0.25\lambda$. It consists of five absorption bands from 0.5THz to 5THz having an absorption rate of 99% on four bands and thus shows a high-sensitivity performance at THz frequencies. To achieve more bandwidth coverage, a tuning mechanism is incorporated into the absorber by the way of including graphene material along the spacings of the convoluted line. The proposed absorbers are having rotational symmetry structures and hence they are polarization insensitive. The parametric analysis was done for all three absorbers to optimize the design. The proposed absorbers with a simple design have potential applications in the field of the medical, military, and civilian sectors.

References

[1] Ming Chen, Chen Chen, Shijie Deng, IEEE Photonics J. **12**(3), 1 (2020).
[2] Amir Ebrahimi, Rajour Tanyi Ako, Wendy S. L. Lee, IEEE Trans. THz Sci. Tech. **10**(2), 19524449 (2020).
[3] Gaurav Varshney, IEEE Sens. J. **21**(2), 15 (2021).
[4] Yue Wang, Dongying Zhu, Zijian Cui, IEEE Trans. THz Sci. Tech, **10**(6), 20114227 (2020).
[5] Somayyeh Asgari, Tapio Fabritius, IEEE Access **10**(63658), 63658 (2022).
[6] Gui-Zhen Wang, Ben-Xin Wang, Journal of Lightwave Techology **33**(24), 5151 (2015).
[7] Balu Ashvanth, Selvi Kanimozhi, Pramana **95**(193), 1 (2021).
[8] Yin Zhang, Yijun Feng, Junming Zhao, Optik-Int. J. Lgt & Elen. Opts. **384**(15), 1 (2020).
[9] Jinzu Jia, Yunpeng Ma, Cong Sun, Optik-Int. J. Lgt & Elen. Opts. **200**(35), 1 (2020).
[10] Da-Wei Wang, Wen-Sheng Zhao, Rui-Zhen Wang, IET Microwaves, Antennas and Propagation **25**(13), 911 (2019).
[11] Jin Huang, Jining Li, Yue Yang, Optica **28**(12), 1 (2020).
[12] Balu Ashvanth, Bactavatchalame Partibane, Govindanarayanan Idayachandran, Bull. Mater. Sci. **281**(44), 1 (2021).
[13] Balu Ashvanth, Bactavatchalame Partibane, M. G. N. Alzath, IEEE Antennas and Wireless Propagation Letters **21**(1), 114 (2022).
[14] Zhiren Li, Yongzhi Cheng, Hui Luo, Fu Chen, Xiangcheng Li, Journal of Alloys and Compounds **925**(5), 1 (2022).
[15] Ben-Xin Wang, Wei Xu, Yangkuan Wu, Nanoscale Advances **106**(5), 1 (2022).
[16] A. Elakkiya, J. Optoelectron. Adv. M. **24**(5-6), 211 (2022).

*Corresponding author: ashvanthece@gmail.com